Research Article | Vol. 28, No. 9 / 27 April 2020 / Optics Express 12771
Optics EXPRESS

Ge-rich graded SiGe waveguides and interferometers from 5 to 11 µm wavelength range

MIGUEL MONTESINOS-BALLESTER,[1,*] VLADYSLAV VAKARIN,[2] QIANKUN LIU,[1] XAVIER LE ROUX,[1] JACOPO FRIGERIO,[1] ANDREA BALLABIO,[3] ANDREA BARZAGHI,[3] CARLOS ALONSO-RAMOS,[1] LAURENT VIVIEN,[1] GIOVANNI ISELLA,[3] AND DELPHINE MARRIS-MORINI[1]

[1] *Université Paris-Saclay, CNRS, Centre de Nanosciences et de Nanotechnologies, 91120 Palaiseau, France*
[2] *Currently in Nexdot, 102 Avenue Gaston Rousssel, Romainville 93230, France*
[3] *L-NESS, dipartimento di Fisica, Politecnico di Milano, Polo di Como, 42 Via Anzani, Como 22100, Italy*
[*] *miguel.montesinos@c2n.upsaclay.fr*

Abstract: The mid-infrared (mid-IR) wavelength range hosts unique vibrational and rotational resonances of a broad variety of substances that can be used to unambiguously detect the molecular composition in a non-intrusive way. Mid-IR photonic-integrated circuits (PICs) are thus expected to have a major impact in many applications. Still, new challenges are posed by the large spectral width required to simultaneously identify many substances using the same photonic circuit. Ge-rich graded SiGe waveguides have been proposed as a broadband platform approach for mid-IR PICs. In this work, ultra-broadband waveguides are experimentally demonstrated within unprecedented wavelength range, efficiently guiding light from 5 to 11 µm. Interestingly, losses from 0.5 to 1.2 dB/cm are obtained between 5.1 and 8 µm wavelength, and values below 3 dB/cm are measured from 9.5 to 11.2 µm wavelength. An increase of propagation losses is seen between 8 and 9.5 µm; however, values stay below 4.6 dB/cm in the entire wavelength range. A detailed analysis of propagation losses is reported, supported by secondary ion mass spectrometry measurement, and different contributions are analyzed: silicon substrate absorption, oxygen impurities, free carrier absorption by residual doping, sidewall roughness and multiphonon absorption. Finally, Mach-Zehnder interferometers are characterized, and wideband operation is experimentally obtained from 5.5 to 10.5 µm wavelength.

1. Introduction

The mid-infrared (mid-IR) wavelength regime, spanning from 2 to 20 µm, has recently gained a great significance in the Photonic Integrated Circuit (PIC) community due to its vast number of applications [1]. As this wavelength range hosts the vibrational and rotational resonances of a large variety of molecules, this so called "fingerprint region" can be used to unambiguously detect a broad number of substances such as carbon dioxide (CO_2), carbon monoxide (CO), methane (CH_4), ammonia (NH_3) or nitrous oxide (N_2O) [2]. The strong and specific absorption of these molecules in the mid-IR range can thus be used to detect small analyte concentrations, potentially up to parts per billion (ppb), having a high impact in sensing and monitoring applications in fields like environmental monitoring [3], hazard detection [4], industrial process control [5], astronomy [6] or non-invasive medical diagnostics [7]. Moreover, the use of mid-IR PICs has also been proposed as a powerful solution to overcome several major existing drawbacks in other important areas such as thermal imaging [8] or optical communications [9,10].

#391464
Journal © 2020
https://doi.org/10.1364/OE.391464
Received 28 Feb 2020; accepted 5 Apr 2020; published 14 Apr 2020

Optics EXPRESS

Among the different materials investigated to develop mid-IR photonic circuits [11–16], germanium (Ge) based circuits benefit from both the compatibility with large scale and high-performance fabrication tools and a wide transparency window, extending up to 15 µm wavelength. Ge-on-silicon (Si) or graded silicon-germanium (SiGe) waveguides have already been successfully developed within the mid-IR spectrum [17–21]. However new challenges arise due to the wide spectral range of mid-IR applications, such as the development of ultrawideband photonic circuits to analyze simultaneously many substances using the same photonic circuit.

In this context, Ge-rich graded SiGe waveguides have been proposed as a broadband platform approach for mid-IR PIC and propagation losses in the range of 2-3 dB/cm, from 5.5 to 8.5 µm have been previously reported [22]. In this work, we demonstrate that these waveguides can be used in an unprecedented wavelength range, from 5 to 11 µm wavelength, providing an analysis of the main sources of propagation losses in an unprecedented wavelength range. Furthermore, the experimental characterization of asymmetric Mach-Zehnder interferometers (MZIs) has been carried out, showing clear interference patterns from 5.5 to 10.5 µm wavelength. These results confirm the wide bandwidth operation of integrated devices based on the Ge-rich SiGe platform.

2. Propagation losses measurement and analysis

2.1. Fabrication and characterization

The Ge-rich graded SiGe platform under study has been previously reported in [22]. It relies on an 11 µm-thick graded SiGe layer epitaxially grown on Si substrate, in which the Ge concentration linearly increases from 0 up to 79%, followed by a 2 µm-thick $Si_{0.2}Ge_{0.8}$ layer (Fig. 1(a)). Low-energy plasma-enhanced chemical vapor deposition is used to grow the $Si_{1-x}Ge_x$ material. The structures are patterned using laser lithography, followed by an inductively coupled plasma, reactive ion etching (ICP-RIE) step. Then, an oxygen-plasma cleaning process, followed by a piranha (H_2O_2 + sulfuric acid) bath are carried out in order to remove any residue from the etching step (Fig. 1(b)). The resulting waveguide etching depth is 6.1 µm and the width is 6.2 µm. 50 µm-wide input/output waveguides are used to butt couple the laser beam in and out of the sample, followed by tapers leading to the 6.2 µm-wide waveguides. It is worth noticing that this design ensures operation over the broad wavelength range investigated in this work.

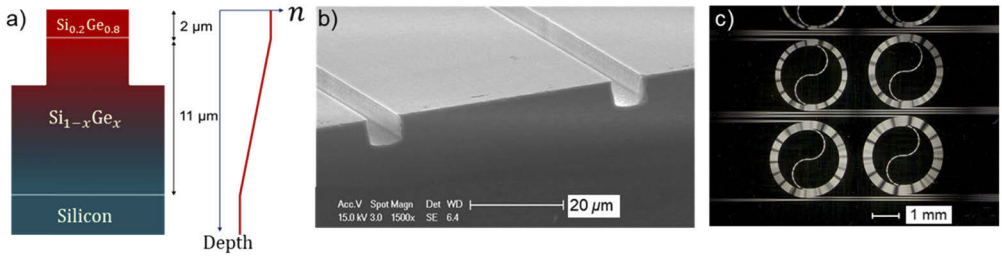

Fig. 1. (a) Graded-index platform scheme and representation of the refractive index (n) linear-increase, as a function of the platform depth. (b) SEM pictures of the sample facet in where the 50-µm-wide input (output) waveguide is shown. (c) Optical microscope picture of spirals fabricated in the sample.

A set of spirals of different lengths have been fabricated, as shown in Fig. 1(c), to extract propagation losses by means of the cutback method. The on-chip propagation length varies up to 14 cm. The free-space characterization setup is based on a tunable Quantum Cascade Laser (QCL). ZnSe aspherical lenses are used to couple the light in and out of the photonic circuit. Waveguide transmission is then measured using a Mercury Cadmium Telluride (MCT) detector. To reduce spectrum oscillations, a Savitzky-Golay filter is applied on the measurement, with 3rd

Optics EXPRESS

polynomial order and scanning over 0.1 µm wavelength range. Finally, the results are plotted in Fig. 2.

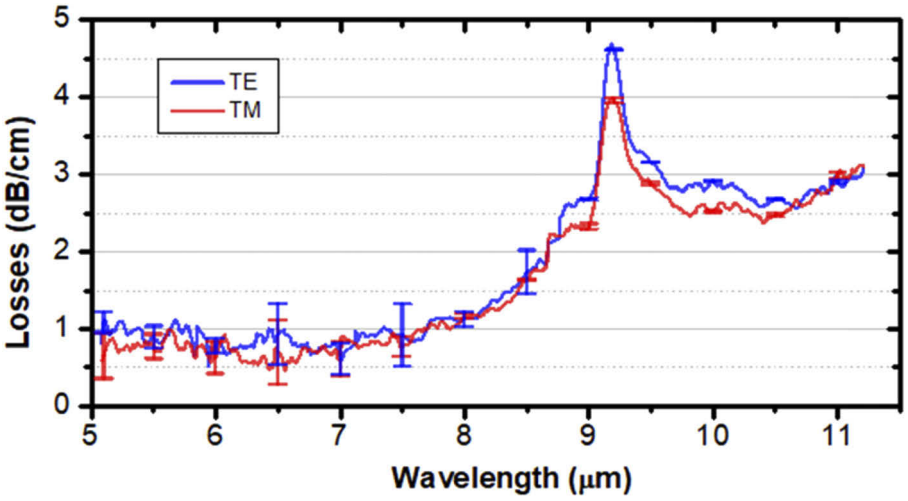

Fig. 2. Propagation losses as a function of the wavelength for TM and TE polarizations. The error bars at different wavelengths have been calculated with the r-squared coefficient of the linear fitting of the cutback method

As it can be seen in Fig. 2, low propagation losses between 0.5 and 1.2 dB/cm are obtained from 5.1 to 8 µm and below 3 dB/cm from 9.5 to 11.2 µm wavelength, for both TE and TM polarization. An increase of propagation losses around 9.2 µm wavelength, reaching 4 dB/cm in TM polarization and 4.6 dB/cm in TE polarization is observed. Interestingly these values are still moderate, and do not prevent the use of these waveguides for many on chip application in the entire range from 5 to 11 µm.

2.2. Analysis

Even if propagation losses from 0.5 to 4.6 dB/cm are appropriate for many on-chip applications, it is interesting to evaluate the origin of these losses for the different wavelength ranges and to investigate possible routes of improvement. Different contributions are analyzed in the following: substrate absorption, oxygen impurities, free carrier absorption by residual doping, sidewall roughness and multiphonon absorption.

Substrate absorption: As Si is known to provide absorption beyond 7 µm wavelength [23], the influence of Si substrate as a possible contribution of optical losses is investigated by mode calculations. Mode profiles are reported in Fig. 3 for TE and TM polarization and for different wavelengths from 5 to 11 µm. In all cases the graded SiGe layer allows to confine the light in the top part of the epitaxial layer, far from the Si substrate. Mode overlap between the guided modes and the substrate is always below 0.01%, making this contribution totally negligible in the measured propagation losses.

Si-O-Si absorption peak ($\lambda = 9.2\,\mu m$): The increase of propagation losses around 9.2 µm wavelength, reaching 4 dB/cm in TM polarization and 4.6 dB/cm in TE polarization is due to optical absorption from the Si-O-Si vibration of interstitial oxygen ($Si:O_i$) [24]. As commonly seen in SiGe alloys, the wavelength of this absorption peak is slightly shifted in comparison with the 1106 cm^{-1} (λ=9.04 µm) absorption peak of Si-O-Si vibration mode in pure Si layers, possibly due to the expansion of Si-Si bonds [25,26] in the SiGe

Optics EXPRESS

matrix. Secondary ion mass spectrometry (SIMS) characterization has been performed to corroborate the analysis. As it can be seen in Fig. 4, the oxygen concentration varies within the epitaxial growth. A constant concentration of 1.5×10^{17}cm^{-3} is measured in the 2 µm-thick $Si_{0.2}Ge_{0.8}$ top layer. Then a peak up to 2.5×10^{17}cm^{-3} is seen at the interface with the graded layer and finally the oxygen concentration decreases when going deeper in the graded SiGe layer. Interestingly, this evolution is compatible with the different values of propagation losses measured between TE and TM polarization. Indeed, the optical mode in TE polarization is more concentrated in the constant composition layer of the waveguide (see Fig. 3), resulting in higher propagation losses.

Free carrier absorption: Residual doping, even at relatively low concentrations, can be responsible of optical losses by free carrier absorption. Residual boron and phosphorous concentration profiles measured by SIMS are reported in Fig. 4. To quantify the effect on the propagation losses, a mean values of 5×10^{14} cm^{-3} for boron and 2×10^{15} cm^{-3} for phosphorous are considered in the following, corresponding to the average values in the 6 µm-thick top layer, where most of the guided mode is confined (See Fig. 3). By compensation, the residual electron concentration is estimated to be 1.5×10^{15} cm^{-3}. Based on this value, the absorption coefficient has been calculated as a function of the wavelength, using the model reported in [27] and later experimentally confirmed in [28]. The corresponding contribution to propagation losses is reported in green in Fig. 5. It varies from 0.2 dB/cm at 5 µm to 1.2 dB/cm at 11.5 µm wavelength.

Lateral sidewall roughness: Sidewall roughness can be responsible for light diffusion and thus propagation losses, especially when using deeply etched waveguides. To evaluate the effect of roughness as a function of the wavelength, the model reported in [29] is used, whose parameters are obtained by fitting the experimental measurement. Indeed, from the different contributions, only free carrier absorption and sidewall roughness influence propagation losses between 5 and 7.5 µm wavelength. Since free carrier absorption contribution is known thanks to the previously reported SIMS characterization, the sidewall roughness parameters (correlation length and roughness standard deviation) can be obtained by fitting the experimentally measured propagation losses. A correlation length of 100 nm is obtained, with a roughness standard deviation of 9 nm. Finally, the sidewalls roughness contribution to propagation losses is reported in violet in Fig. 5.

Multiphoton absorption: Multiphonon absorption is responsible for absorption above 8 µm (resp. 14 µm) wavelength in Si (resp. Ge) [23,30]. Even though infrared absorption spectra of crystalline SiGe alloys have been reported with different Si content [25], a detailed study of multiphonon absorption for Ge-rich SiGe alloys in the 8-11 µm wavelength range is missing in the literature. However, from Fig. 5, it is possible to evaluate the contribution of multiphonon absorption as the difference between the experimental measurement and the sum of the contributions from the lateral sidewall roughness and free carrier absorption (except at the 9.2 µm absorption peak). Using this method, it can be estimated that the multiphonon processes in the top $Si_{0.2}Ge_{0.8}$ and in the graded SiGe layers are responsible for around 1.5 dB/cm increase of the propagation loss beyond 8 µm wavelength

As a conclusion, it can be deduced that the main contributions of the waveguide propagation losses strongly depend on the wavelength. At wavelengths lower than 8 µm, a combination of sidewall roughness and free carrier absorption is the responsible for propagation losses, with values lower than 1.2 dB/cm obtained for both polarizations. On the other hand, for wavelengths larger than 8 µm, both multiphonon and free carrier absorption contribute to the propagation losses. Nevertheless, propagation losses below 3 dB/cm is obtained from 9.5 to 11 µm wavelength. Finally, around 9.2 µm wavelength, interstitial oxygen absorption is responsible for an increase of

Optics EXPRESS

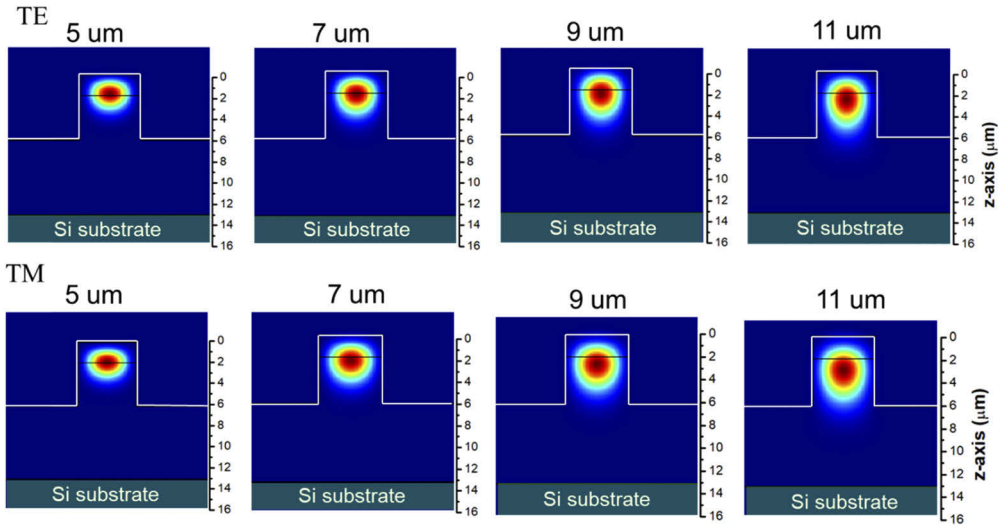

Fig. 3. Optical power distribution in the waveguide for TE and TM polarization at different wavelengths: 5, 7, 9, and 11 μm reported on top of each mode calculation. In dark green shading is shown the Si substrate.

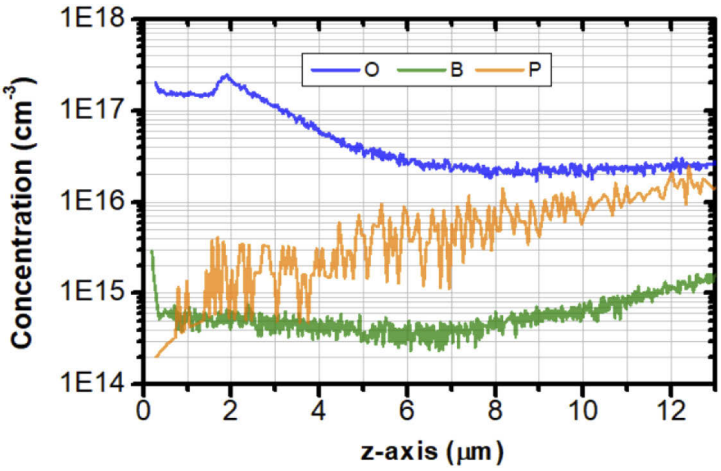

Fig. 4. Oxygen (blue), Boron (green) and Phosphorous (yellow) concentration as a function of the z-axis direction calculated by SIMS characterization of the sample.

the propagation losses up to 4.6 dB/cm. As possible optimization, a modification of the epitaxial growth deposition system is envisioned in the future to reduce the oxygen impurity concentration. Furthermore, by decreasing the main residual doping concentration, or by a fine tuning of the doping compensation effect, a reduction of free carrier absorption can be expected. An additional reduction of propagation losses can be obtained by increasing the Ge content in the graded buffer and constant composition layer. This should strongly reduce multiphonon absorption in the 8 to 11 μm region as well as the Si:O:S_i peak. Thus, propagation losses around 2 dB/cm can be expected from 8 to 11 μm wavelength (1.5 dB/cm for multiphoton absorption plus 0.5 dB/cm for dopants and roughness). To optimize propagation losses in the lowest wavelength range, the influence of waveguide roughness must be decreased. For this, both an improvement of waveguide definition and etching, or the use of wider waveguide to reduce the overlap of the

Optics EXPRESS

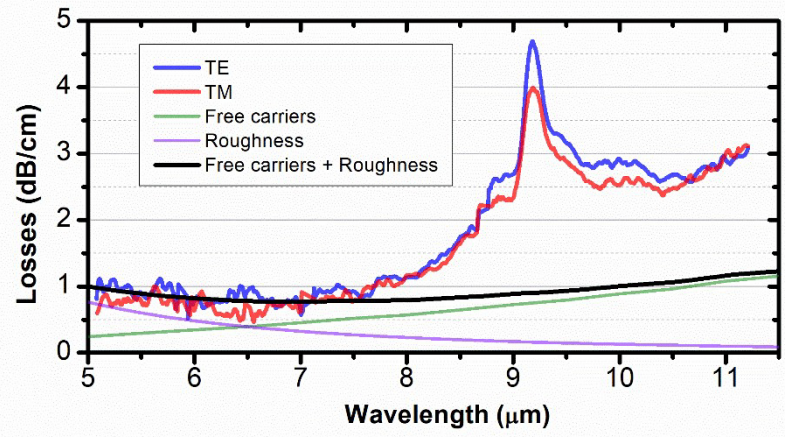

Fig. 5. Waveguide propagation loss: contribution from free carrier absorption (green), sidewall roughness (violet), the sum of these two contributions (black). Experimentally measured TE (blue) and TM (red) propagation losses are also plotted.

guided mode with the sidewalls can be envisioned. When combined with a reduction of residual doping, low loss below 0.5 dB/cm can be expected from 5 to 8 μm wavelength.

3. Wideband Mach Zehnder interferometer

To date, the Ge-rich $Si_{1-x}Ge_x$ graded platform is the only waveguide platform operating in a wide wavelength range, from 5 to 11 μm, using a single waveguide design. Even though single mode condition is not fulfilled in such a wide wavelength range, we demonstrate below the potential of this platform to develop wideband integrated devices. Indeed, while Mach Zehnder interferometers, resonators and Fourier transform spectrometers operating between 5 and 8.5 μm have been reported previously [31–33], we extend here the characterization of MZIs to larger wavelengths. To this end, asymmetric MZIs with arm length unbalances of 47 and 84.6 μm are used. The measurement is done in TM polarization and the MZIs transmission measurements are normalized by the transmission of a straight waveguide on the chip, in order

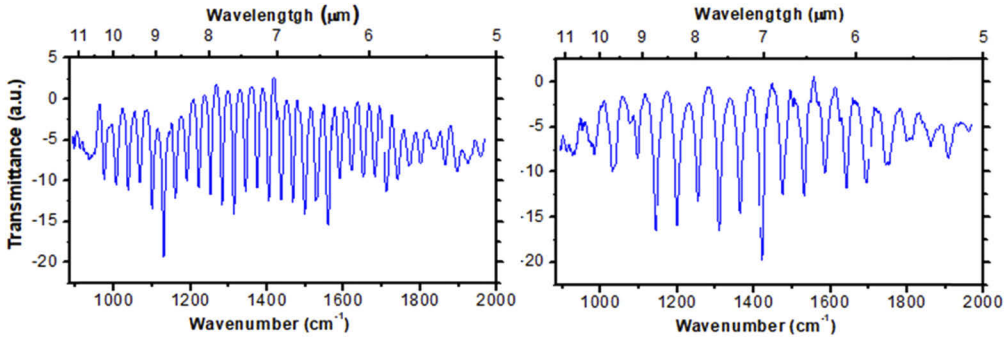

Fig. 6. Transmission of asymmetric Mach Zehnder interferometer normalized by straight waveguide as a function of the wavenumber (bottom x-axis) or wavelength (top x-axis) of (a) MZI with $\Delta L = 47$ μm and (b) MZI with $\Delta L = 84.6$ μm. The data has been smoothed by a Savitzky-Golay filter, taking 20 samples (i.e. 0.1 μm range) and a 4^{th} order filter.

Optics EXPRESS

to obviate atmospheric absorption peaks, the wavelength response of the characterization laser and coupling and propagation losses. As previously done, a 4th polynomial Savitzky-Golay filter has been implemented with 0.1 µm wavelength span on the measurement. In Fig. 6 are plotted the normalized transmission of both MZIs as a function of the wavenumber (bottom x-axis) or wavelength (top x-axis). In both cases the resonances are clearly seen for a wavelength range spanning from 5.5 to 10.5 µm. This measurement confirms the wideband operation of the multi-mode interferometer (MMI) used as splitter and combiner with a very good matching with MMI simulation reported previously [31]. Furthermore, this result also demonstrates that even if multimode waveguides are used, the device does not suffer from light coupling to higher order modes.

4. Conclusion

In summary, it is experimentally demonstrated that Ge-rich graded SiGe waveguides can be used in an unprecedented wavelength range, from 5 to 11 µm wavelength, which is a unique feature of the graded index profile in the SiGe waveguide. Propagation losses from 0.5 to 1.2 dB/cm is obtained between 5.1 and 8 µm wavelength, and values below 3 dB/cm are measured from 9.5 to 11.2 µm wavelength. Interestingly losses values stay below 4.6 dB/cm in the entire wavelength range from 5 to 11 µm, for both TE and TM polarizations. A detailed analysis of propagation losses is reported, showing that: (i) the values are compatible with free carrier concentrations below 10^{15} cm^{-3}, (ii) the losses of Si substrate are completely negligible due to the low overlap of the guided mode with the substrate, (iii) the main contribution for sidewall roughness appear in the low wavelength range, (iv) multiphoton absorption in the $Si_{1-x}Ge_x$ alloy contribute to the waveguide propagation losses beyond 8 µm wavelength, (v) the absorption around 9.2 µm wavelength is attributed to oxygen impurities.

Moreover, the characterization of MZI is reported, showing that (i) MMI based splitter and combiner are operating in a wide spectral range from 5.5 to 10.5 µm, which is a unique advantage of the low dispersion within Ge-rich graded SiGe waveguide, (ii) even if the waveguides are not single mode in the entire wavelength range, efficient interferometers are achieved, showing that the devices do not suffer from light coupling to higher order modes. These results pave the way towards the demonstration of efficient mid-IR PICs for a wide range of applications.

Funding

European Research Council (ERC) under the European Union's Horizon research and innovation program (N°-639107-InsPIRE); EU Horizon-2020 FET microSPIRE project (N° 766955).

Acknowledgements

The fabrication of the device was partially performed at the Plateforme de Micro-NanoTechnologie/C2N, which is partially funded by the "Conseil Général de l'Essonne." This work was partly supported by the French RENATECH network. PoliFAB is acknowledged for waveguides fabrication.

Disclosures

The authors declare no conflicts of interest.

References

1. R. Soref, "Mid-infrafred photonics in silicon and germanium," Nat. Photonics **4**(8), 495–497 (2010).
2. I. E. Gordon, L. S. Rothman, C. Hill, R. V. Kochanov, Y. Tan, P. F. Bernath, M. Birk, V. Boudon, A. Campargue, K.V. Chance, B. J. Drouin, J.-M. Flaud, R. R. Gamache, J. T. Hodges, D. Jacquemart, V. I. Perevalov, A. Perrin, K.P. Shine, M.-A. H. Smith, J. Tennyson, G. C. Toon, H. Tran, V. G. Tyuterev, A. Barbe, A. G. Császár, V. M. Devi, T. Furtenbacher, J. J. Harrison, J.-M. Hartmann, A. Jolly, T. J. Johnson, T. Karman, I. Kleiner, A. A. Kyuberis, J. Loos, O. M. Lyulin, S. T. Massie, S. N. Mikhailenko, N. Moazzen-Ahmadi, H. S. P. Müller, O. V. Naumenko, A. V.

Optics EXPRESS

Nikitin, O. L. Polyansky, M. Rey, M. Rotger, S. W. Sharpe, K. Sung, E. Starikova, S. A. Tashkun, J. V. Auwera, G. Wagner, J. Wilzewski, P. Wcisło, S. Yu, and E. J. Zak, "The HITRAN2016 molecular spectroscopic database," J. Quant. Spectrosc. Radiat. Transfer **203**, 3–69 (2017).

3. A. P. Michel, D. J. Miller, K. Sun, L. Tao, L. Stanton, and M. Zondlo, "Long-Path Quantum Cascade Laser–Based Sensor for Methane Measurements," J. Atmos. Oceanic Technol. **33**(11), 2373–2384 (2016).
4. Y. C. Chang, P. Wägli, V. Paeder, A. Homsy, L. Hvozdara, P. van der Wal, J. Di Francesco, N. F. de Rooij, and H. Peter Herzig, "Cocaine detection by a mid-infrared waveguide integrated with a microfluidic chip," Lab Chip **12**(17), 3020–3023 (2012).
5. U. Willer, M. Saraji, A. Khorsandi, P. Geiser, and W. Schade, "Near- and mid-infrared laser monitoring of industrialprocesses, environment and security applications," Opt. Laser Eng. **44**(7), 699–710 (2006).
6. L. Labadie and O. Wallner, "Mid-infrared guided optics: a perspective for astronomical instrumentations,"," Opt. Express **17**(3), 1947–1962 (2009).
7. R. Anty, M. Morvan, M. Le Corvec, C. M. Canivet, S. Patouraux, J. Gugenheim, S. Bonnafous, B. Bailly-Maitre, O. Sire, H. Tariel, J. Bernard, T. Piche, O. Loréal, J. Aron-Wisnewsky, K. Clément, A. Tran, A. Iannelli, and P. Gual, "The mid-infrared spectroscopy: A novel non-invasive diagnostic tool for NASH diagnosis in severe obesity," JHEP Reports (2019).
8. D. Zhang, C. Li, C. Zhang, M. N. Slipchenko, G. Eakins, and J.-X. Cheng, "Depth-rsolved mid-infrered photothermal imaging of living cells and organisms with submicrometer spatial resolution," Sci. Adv. **2**(9), e1600521 (2016).
9. Y. Su, W. Wang, X. Hu, H. Hu, X. Huang, Y. Wang, J. Si, X. Xie, B. Han, H. Feng, Q. Hao, G. Zhu, T. Duan, and W. Zhao, "10 Gpbs DPSK transmission over free-space link in the mid-infrered," Opt. Express **26**(26), 34515–34528 (2018).
10. G. Z. Mashanovich, W. Cao, Z. Qu, K. Li, D. Thomson, M. Nedeljkovic, D. Hagan, and A. Knights, "Mid-Infrared Silicon Photonics for Communications," IJEEC **3**(1), 32–36 (2019).
11. G. Z. Mashanovich, M. M. Milošević, M. Nedeljkovic, N. Owens, B. Xiong, E. J. Teo, and Y. Hu, "Low loss silicon waveguides for the mid-infrered," Opt. Express **19**(8), 7112–7119 (2011).
12. S. A. Miller, M. Yu, X. Ji, A. G. Griffith, J. Cardenas, A. L. Gaeta, and M. Lipson, "Low-loss silicon platform for broadband mid-infrared photonics," Optica **4**(7), 707–712 (2017).
13. L. He, Y. Guo, Z. Han, K. Wada, L. C. Kimerling, J. Michel, A. M. Agarwal, G. Li, and L. Zhang, "Loss reduction of silicon-on-insulator waveguides for deep mid-infrared applications," Opt. Lett. **42**(17), 3454–3457 (2017).
14. Z. Cheng, X. Chen, C. Y. Wong, K. Xu, and H. K. Tsang, "Mid-infrared suspended membrane waveguide and ring resonator on silicon-on-insulator," IEEE Photonics J. **4**(5), 1510–1519 (2012).
15. J. S. Penadés, A. Sánchez-Postigo, M. Nedeljkovic, A. Ortega-Moñux, J. G. Wangüemert-Pérez, Y. Xu, R. Halir, Z. Qu, A. Z. Khokhar, A. Osman, W. Cao, C. G. Littlejohns, P. Cheben, I. Molina-Fernández, and G. Z. Mashanovich, "Suspended silicon waveguides for long-wave infrared wavelengths," Opt. Lett. **43**(4), 795–798 (2018).
16. T. Baehr-Jones, A. Spott, R. Ilic, A. Spott, B. Penkov, W. Asher, and M. Hochberg, "Silicon-on-sapphire integrated waveguides for the mid-infrared," Opt. Express **18**(12), 12127–12135 (2010).
17. Y. C. Chang, V. Paeder, L. Hvozdara, J. M. Hartmann, and H. P. Herzig, "Low-loss germanium strip waveguides on silicon for the mid-infrared," Opt. Lett. **37**(14), 2883–2885 (2012).
18. M. Nedeljkovic, J. S. Penades, V. Mittal, G. S. Murugan, A. Z. Khokhar, C. LittleJohns, L. G. Carpenter, C. B. E. Gawith, J. S. Wilkinson, and G. Mashanovich, "Germanium-on-silicon waveguides operating at mid-infrared wavelengths up to 8.5 µm," Opt. Express **25**(22), 27431 (2017).
19. K. Gallacher, R. W. Millar, U. Griškevičiūte, L. Baldassarre, M. Sorel, M. Ortolani, and D. J. Paul, "Low loss Ge-on-Si waveguides operating in the 8–14 µm atmospheric transmission window," Opt. Express **26**(20), 25667–25675 (2018).
20. M. Brun, P. Labeye, G. Grand, J. M. Hartmann, F. Boulila, M. Carras, and S. Nicoletti, "Low loss SiGe graded index waveguides for mid-IR applications," Opt. Express **22**(1), 508–518 (2014).
21. M. Sinobad, C. Monat, B. Luther-davies, P. Ma, S. Madden, D. Moss, A. Mitchell, D. Allioux, R. Orobtchouk, S. Boutami, J. Hartmann, J. Fedeli, and C. Grillet, "Mid-infrared octave spanning supercontinuum generation to 8.5 µm in silicon-germanium waveguides," Optica **5**(4), 360–366 (2018).
22. J.-M. Ramirez, Q. Liu, V. Vakarin, J. Frigerio, A. Ballabio, X. Le Roux, D. Bouville, L. Vivien, G. Isella, and D. Marris-Morini, "Graded SiGe waveguides with broadband low-loss propagation in the mid infrared," Opt. Express **26**(2), 870–877 (2018).
23. F. A. Johnson, "Lattice absorption bands in silicon," Proc. Phys. Soc., London **73**(2), 265–272 (1959).
24. E. Artacho, F. Ynduráin, B. Pajot, R. Ramírez, C. P. Herrero, L. I. Khirunenko, K. M. Itoh, and E. E. Haller, "Interstitial oxygen in germanium and silicon," Phys. Rev. **56**(7), 3820–3833 (1997).
25. I. Yonenaga, M. Nonaka, and N. Fukata, "Interstitial oxygen in GeSi alloys," Phys. B **308-310**, 539–541 (2001).
26. M. Lorenc and J. Humlicek, "Vibrational modes in Si_xGe_{1-x} alloys: temperature and compositional dependences," Acta Phys. Pol., A **92**(5), 899–902 (1997).
27. M. Nedeljkovic, R. Soref, and G. Z. Mashanovich, "Predictions of Free-Carrier Electroabsorption and Electrorefraction in Germanium," IEEE Photonics J. **7**(3), 1–14 (2015).
28. M. Montesinos-Ballester, V. Vakarin, J. M. Ramirez, Q. Liu, C. Alonso-Ramos, X. L. Roux, J. Frigerio, A. Ballabio, A. Barzaghi, L. Deniel, D. Bouville, L. Vivien, G. Isella, and D. Marris-Morini, "Optical modulation in Ge-rich SiGe waveguides in the mid-IR wavelength range up to 11 µm," arXiv:1911.10827, (2019).

Optics EXPRESS

29. F. P. Payne and J. P. R. Lacey, "A theoretical analysis of scattering loss from planar optical waveguides," Opt. Quantum Electron. **26**(10), 977–986 (1994).
30. S. J. Fray, F. A. Johnson, J. E. Quarrington, and N. Williams, "Lattice bands in germanium," Proc. Phys. Soc., London **85**(1), 153–158 (1965).
31. V. Vakarin, J.-M. Ramírez, J. Frigerio, A. Ballabio, X. Le Roux, Q. Liu, D. Bouville, L. Vivien, G. Isella, and D. Marris-Morini, "Ultra-wideband Ge-rich silicon germanium integrated Mach-Zehnder interferometer for midinfrared spectroscopy," Opt. Lett. **42**(17), 3482–3485 (2017).
32. J. M. Ramírez, Q. Liu, V. Vakarin, X. L. Roux, J. Frigerio, A. Ballabio, C. Alonso-Ramos, E. Simola, L. Vivien, G. Isella, and D. Marris-Morini, "Broadband integrated racetrack ring resonators for long-wave infrared photonics," Opt. Lett. **44**(2), 407 (2019).
33. Q. Liu, J. M. Ramírez, V. Vakarin, X. L. Roux, C. Alonso-Ramos, J. Frigerio, A. Ballabio, E. Simola, D. Bouville, L. Vivien, G. Isella, and D. Marris-Morini, "Integrated broadband dual-polarization Ge-rich SiGe mid-infrared Fourier-transform spectrometer," Opt. Lett. **43**(20), 5021 (2018).